

Improvement of 3D Point Cloud Alignment for Super-Resolution Applications

Keisuke Myosen*, Tomoyuki Takanashi*, Midori Tanaka** and Takahiko Horiuchi*;

* Graduate School of Science and Engineering, Chiba University, Chiba, Japan

** Graduate School of Global and Transdisciplinary Studies, Chiba University, Chiba, Japan

Abstract

With the prevalence of 3D scanners and 3D printers, manufacturing various 3D objects has become easier in recent years. When measuring the surface shape of an object using a 3D scanner, it is desirable to perform measurements at the highest possible resolution. However, there are many objects for which the resolution of commercial 3D scanners is insufficient. One solution to this problem is to apply super-resolution technology by measuring 3D data multiple times. It is crucial to align the 3D point clouds generated by multiple measurements accurately, but the conventional alignment methods are not accurate enough. This study aimed to improve the accuracy of the alignment process for 3D point clouds. The proposed method consists of the following four steps: (1) 3D point clouds are adaptively sampled. (2) A fast point feature histogram is used to extract features from the sampled point clouds. (3) The random sample consensus method is used to estimate an initial alignment. (4) The iterative closest point method is used to perform a precise alignment procedure. The feasibility of the proposed method is verified through experiments using real objects.

Introduction

In recent years, 3D scanners and 3D printers have become more popular. Consequently, manufacturing using 3D printers has become easier for companies and individuals. In general, there are two main approaches to forming a desired object using a 3D printer. One is to use a design tool (such as computer-aided design software), and the other is to capture information from a real object. In the latter case, 3D scanners play a crucial role in performing sophisticated object analysis. The accuracy of 3D scanners has improved dramatically in recent years. Popular instruments have traditionally used monocular cameras. However, such instruments require long measurement times. In recent years, active measurement instruments using stereo cameras have emerged, which has significantly reduced measurement times.

To represent the appearance of an object accurately, it is important to measure and reproduce small irregularities and textures on the surface of the object. For example, the width of a cloth fiber is typically approximately 0.01 mm. Therefore, to capture the appearance of cloth on a 3D object, it is necessary to capture data with a very high resolution. However, very few commercial 3D scanner products can perform measurements at sufficiently high resolutions.

As an approach to increasing resolution, some studies have adopted super-resolution techniques. Schultz et al. implemented super-resolution for 2D images using a Bayesian maximum a posteriori probability estimation technique that minimizes assessment functions corresponding to posterior probabilities based on the continuity of several 2D images [1]. However, such methods cannot implement super-resolution for 3D data. Schuon et

al. proposed an approach for obtaining high-resolution 3D data by super-resolving depth images [2]. However, their approach adopted super-resolved depth images captured from a particular direction, meaning arbitrary 3D data could not be super-resolved. In a study on alignment processes for 3D data, Makadia et al. proposed an approach to correct the alignment of scanned data automatically with little overlap [3]. Their study mainly focused on producing a single omnidirectional 3D representation from several scanned datasets. However, because a large portion of the 3D data used in super-resolution techniques overlap and differ in terms of sampling locations, it is difficult to apply the alignment procedure described above to generalized super-resolution techniques.

In this study, we aim to improve the alignment accuracy of 3D point clouds for super-resolution techniques.

Proposed method

An outline of the processing steps of the proposed method is presented in Fig. 1, and consists of the following four steps: (1) 3D point clouds are adaptively sampled. (2) A fast point feature histogram (FPFH) is used to extract features from the sampled point clouds. (3) The random sample consensus (RANSAC) method is used to estimate an initial alignment. (4) The iterative closest point (ICP) method is used to perform a precise alignment procedure.

Adaptive sampling

In the first step, point clouds are adaptively sampled according to their importance for alignment processing.

In the alignment of 3D point clouds, regions with locally uniform normals (such as planes) tend to fall into local optimal solutions, leading to decreased accuracy. Therefore, we extract regions in which normals are locally uniform and down-sample the point clouds associated with those regions. In this study, we extracted regions based on the method described in [4] as follows:

1. Specify the thresholds of curvature r_{th} and smoothness θ_{th} .
2. During region expansion, soft point clouds $P = \{p_i\}$ by the curvature values of their corresponding normal vectors to identify a seed point p_0 with the minimum curvature. Find the 30 nearest neighbors of the current seed point p_0 .
3. If the angle between the normal n_0 of p_0 and the normal n_j of a nearby point p_j satisfies $\|n_0 \cdot n_j\| > \cos \theta_{th}$, then add point p_j to the current region. If the curvature of the point p_j is less than r_{th} , then add the point to the list of potential seed points. Perform this process for all 30 nearest neighbors.
4. If the potential seed point list is not empty, set the current seed to the next available seed and return to Step 2.
5. Add the current region to the segmentation results and return to Step 2.
6. Return the segmentation results.

Among the segmented regions, regions with large areas become target regions for down-sampling. In this study, down-sampling was performed by using the center of gravity of the voxel in the target area as a representative point.

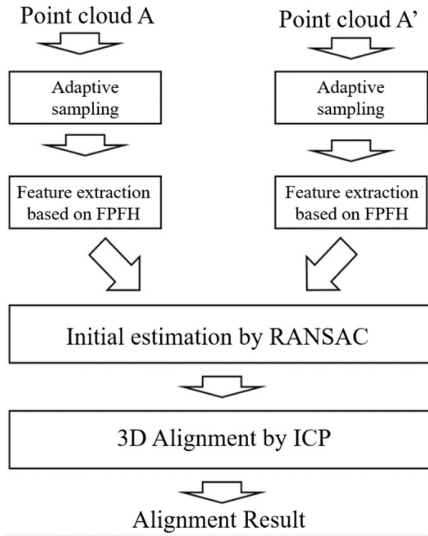


Figure 1. Processing steps used by the proposed method.

Feature Extraction based on FPFH

In this section, we will explain a feature extraction method of the down-sampled 3D data based on FPFH [5]. FPFH improved the calculation speed of point feature histograms (PFH) method [6]. How to find the PFH of a point p_q in the sampled point cloud P is as follow: 1. for each point p_q , all of p_q 's neighbors enclosed in the sphere with a given radius r are selected (k -neighborhood); 2. for every pair of points p_i and p_j ($i \neq j$) in the k -neighborhood of p_q and their estimated normals n_i and n_j , we define a Darboux uvn frame ($u = n_i, v = (p_j - p_i) \times u, w = u \times v$) and compute these three angular variations of n_i and n_j as follows:

$$\alpha = v \cdot n_j \quad (1)$$

$$\varphi = \frac{u \cdot (p_j - p_i)}{\|(p_j - p_i)\|} \quad (2)$$

$$\theta = \arctan(w \cdot n_j, u \cdot n_j) \quad (3)$$

An influence region diagram illustrating FPFH computation is presented in Fig. 2. Eventually, features are outputted as a feature point cloud P_F . This process is also applied to another point cloud Q, resulting in a feature point cloud Q_F . Next, initial alignment estimation is performed using the feature point clouds P_F and Q_F .

Initial Estimation using RANSAC

This section describes how we compute initial position estimates for the ICP method using an FPFH. To derive initial estimates from FPFHs, RANSAC [7] was adopted in this study. The point clouds PQ and feature point clouds $P_F Q_F$ are the inputs for RANSAC. RANSAC estimates a 3D affine transformation matrix T_0 that minimizes the sum of squared distances between each point $p \in P$ and the corresponding points $q \in Q$ as follows:

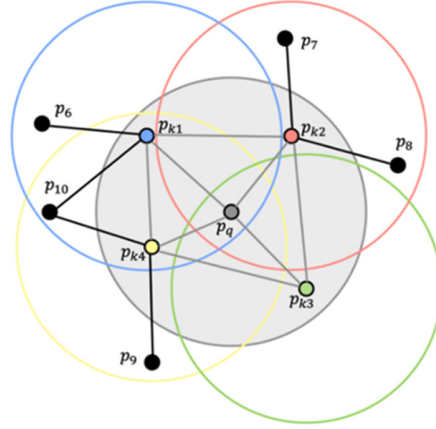


Figure 2. Influence region diagram for an FPFH.

$$T_0 = \underset{T}{\operatorname{argmin}} \varepsilon(T) = \underset{T}{\operatorname{argmin}} \sum_{p \in P} (Tp - q)^2 \quad (4)$$

The RANSAC algorithm can be summarized as follows.

1. Find n random points in the point cloud P and the corresponding points in Q using the feature point clouds P_F and Q_F obtained by an FPFH.
2. If the Euclidean distance between corresponding points is greater than a threshold, return to Step 1.
3. Estimate a 3D affine transformation matrix T_0 using n sampled correspondences.
4. Apply the matrix T_0 to transform the point cloud P.
5. Find inlier points by performing a spatial nearest neighbor search between the transformed points and the point cloud Q, followed by Euclidean thresholding. If the number of inliers is too low, return to Step 1.
6. Re-estimate a 3D affine transformation matrix based on the inlier point correspondences. Measure $\varepsilon(T_0)$ using the inliers. If this measurement results in the smallest value thus far, then set T_0 to the resulting transformation matrix.

3D Alignment using ICP

In this section, we describe a 3D alignment method based on ICP [8]. For this process, the initial matrix derived in Sec. 2.3 and each point cloud are used as inputs. In its simplest form, the ICP algorithm iterates using two steps. Beginning with an initial estimate of the alignment parameters T_0 , the algorithm forms a sequence of estimates T_k that progressively reduce errors. Each iteration of the algorithm consists of the following two steps:

$$\varphi = \underset{q \in Q}{\operatorname{argmin}} \varepsilon^2(|q - T_k(p)|) \quad p \in P \quad (5)$$

$$T_{k+1} = \underset{T}{\operatorname{argmin}} \sum_{p \in P} \varepsilon^2(|q_\varphi - T(p)|) \quad (6)$$

Here, correspondence is denoted by the function φ . For each data point, this function selects the corresponding point in another point cloud. ε^2 denotes Euclidean distance in the form of an error function. One can see that both steps reduce the error and that the error is bounded from below. Therefore, convergence to a local minimum is guaranteed. Furthermore, it is straightforward to discern a termination criterion. When the set of correspondences

does not change in the first step, the value of T_{k+1} will be set equal to T_k in the second step, meaning no further change is possible.

The final result obtained by the proposed alignment method is a 3D affine transformation matrix T_k .

Experiments

To verify the proposed method, we conducted evaluation experiments using real objects. In this section, we describe the measurement method and acquired point cloud data, as well as experimental results. In our experiment, we used a threshold of $r_{th} = 1.0$ and θ_{th} was varied from $\pi/180$ to $3\pi/180$ based on empirical observations. The voxel size for adaptive sampling was set to 9 mm (real size).

Measurement

Figure 3 presents the test samples used in our experiments. Each object in Fig. 3 is characterized by many planar regions or repeating patterns. The measurement system used for our experiments was an HP 3D Structured Light Scanner Pro 3. This system can collect 3D data at resolutions up to 0.05 mm. The specifications of the measurement system are listed in Table 1. For measurement, 3D object data were obtained by synthesizing data measured four times at 90° intervals using a 360° rotation table. The data were outputted in the PLY 3D format.

The measurement environment is presented in Fig. 4. We assumed that the collected data would be used for super-resolution applications. Therefore, the sampling position was shifted for each measurement. In our measurements, we moved and rotated each object appropriately so the sampling position did not return to the first measurement position. Table 2 lists the data collected from the test samples.

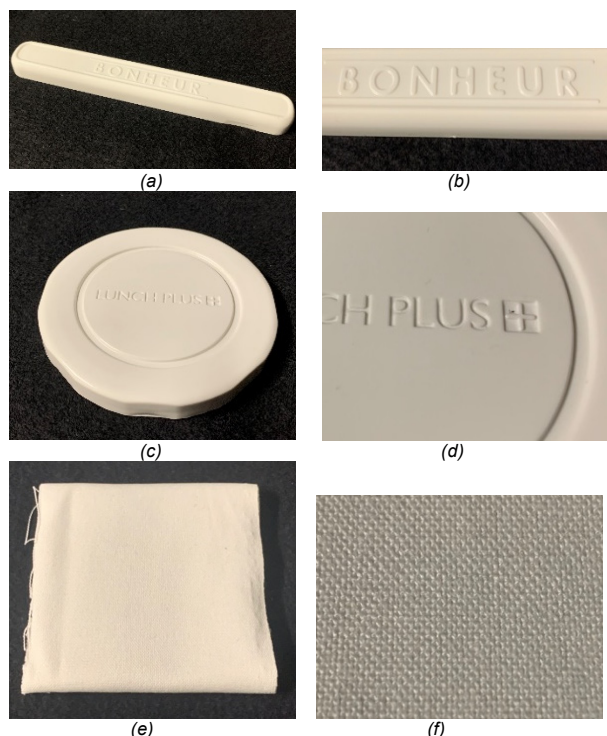


Figure 3. Test samples. (a) Object containing many planes, (b) magnified view of (a) (c) another object with many planes, (d) magnified view of (c), (e) object containing repeating patterns, and (f) magnified view of (e).

Table 1. Specifications of the 3D scanner

	3D Structured Light Scanner Pro
Measurement method	Pattern optical projection camera method
Maximum resolution	0.05 mm
Measuring speed	2s per scan
Output format	OBJ, PLY, STL

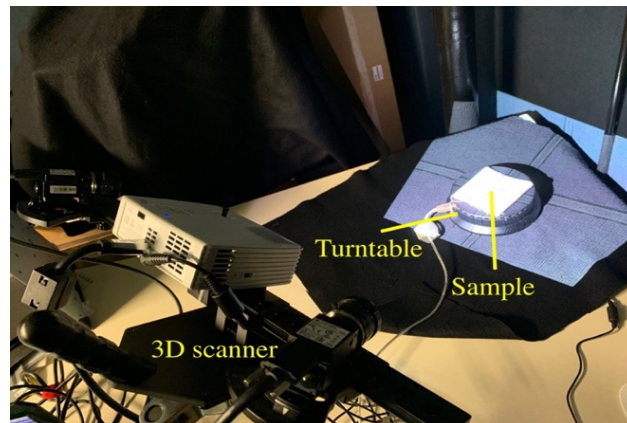


Figure 4. Measurement environment.

Table 2. Data sizes and numbers of points collected from the test samples

	Data sizes	Numbers of points
Fig. 3(a)	94,768 KB	824,440
Fig. 3(b)	98,760 KB	1,266,897
Fig. 3(c)	100,887 KB	1,273,444

Experimental Results

The experimental results for the test samples are presented in Figs. 5 to 7. Figure 5 presents the results for the object in Fig. 3(a). This object has a long stick shape with letters on its surface. Therefore, as shown in Figs. 5(b) and 5(c), the corresponding initial positions in Fig. 5(a), which are indicated by blue and orange, respectively, can be easily aligned without performing adaptive sampling. Fig. 5(d) presents a point cloud after adaptive sampling. One can see that the points on the plane are relatively coarse. As shown in Figs. 5(e) and 5(f), with adaptive sampling, alignment can still be performed with sufficient accuracy.

Figure 6 presents the results for the object in Fig. 3(b). The surface of this object has many planar regions and a circular shape. Therefore, sampling is likely to fall into local optimal solutions. As shown in Figs. 6(b) and 6(c), when adaptive sampling is not performed with respect to the initial position in Fig. 6(a), alignment fails. Fig. 6(d) presents a point cloud after adaptive sampling. It can be confirmed that the points on the plane are relatively coarse. As shown in Figs. 6(e) and 6(f), by performing adaptive sampling, alignment can be performed with sufficient accuracy.

Figure 7 presents the results for the object in Fig. 3(c). The surface of this object has an irregular texture pattern. Therefore, sampling is likely to fall into local optimal solutions. As shown in Figs. 7(b) and 7(c), if adaptive sampling is not performed with respect to the initial position in Fig. 7(a), alignment fails. Fig. 7(d) presents a point cloud following adaptive sampling. Some points

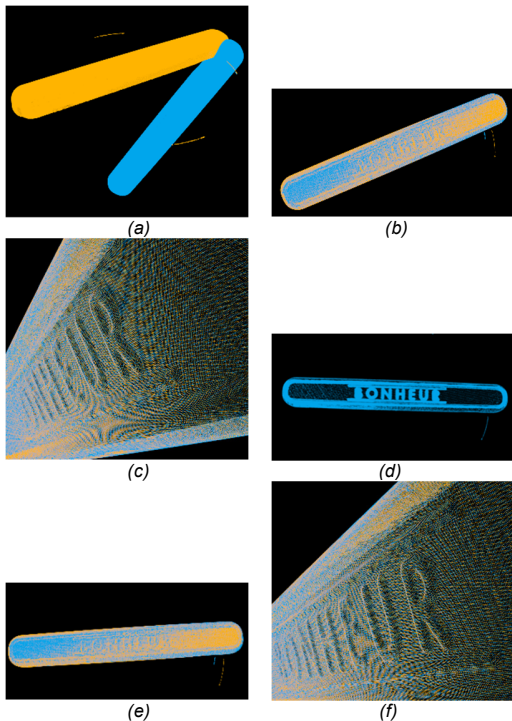


Figure 5. Experimental results for the object in Fig. 3(a). (a) Initial position, (b) results without adaptive sampling, (c) magnified view of (b), (d) point cloud with adaptive sampling, (e) final results with adaptive sampling, and (f) magnified view of (e).

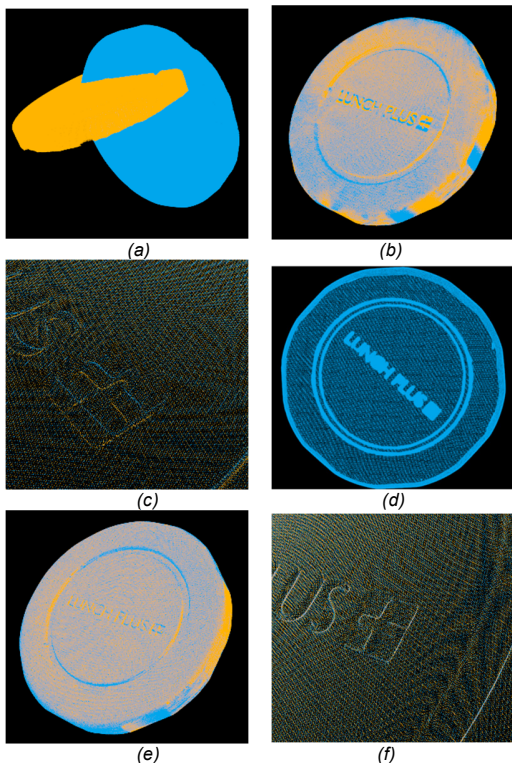


Figure 6. Experimental results for the object in Fig. 3(b). (a) Initial position, (b) results without adaptive sampling, (c) magnified view of (b), (d) point cloud with adaptive sampling, (e) final results with adaptive sampling, and (f) magnified view of (e).

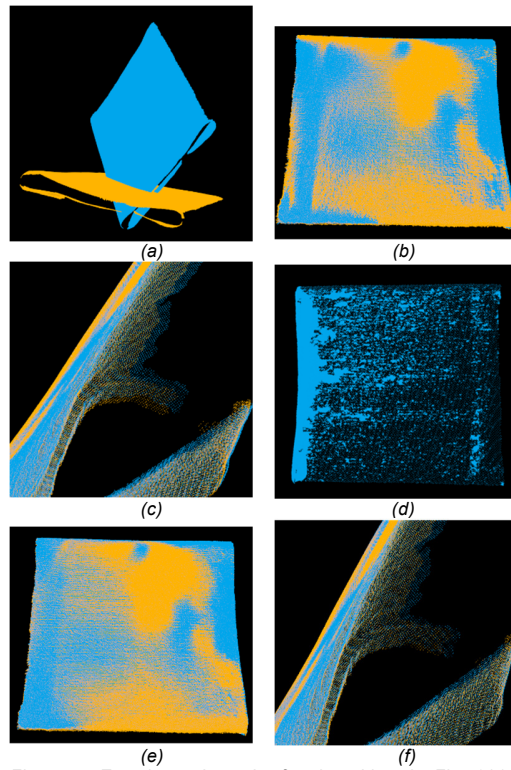


Figure 7. Experimental results for the object in Fig. 3(c). (a) Initial position, (b) results without adaptive sampling, (c) magnified view of (b), (d) point cloud with adaptive sampling, (e) final results with adaptive sampling, (f) magnified view of (e).

are relatively coarse and unstable. As shown in Figs. 7(e) and 7(f), even when adaptive sampling is performed, alignment fails.

Conclusion

In this study, we improved the alignment accuracy of 3D point clouds for 3D super-resolution applications. The proposed method consists of four steps: adaptive sampling, feature extraction, initial estimation, and final alignment. For adaptive sampling, we selectively down-sampled points that were not important for alignment. Real sample measurement and alignment experiments demonstrated that it is possible to avoid local optimal solutions for objects with severe local normal alignment, and the effectiveness of adaptive sampling was confirmed.

In objects such as fabrics with repeated patterns, even if the proposed method is applied, it is still easy to fall into local optimal solutions. Future research will focus on improving alignment accuracy for such objects.

References

- [1] R.R. Schultz and R.I. Stevenson, "Extraction of high-resolution frames from video sequences," IEEE Trans. image processing, vol. 5, issue 6, pp. 996-1011, 1996.
- [2] S. Schuon, C. Theobalt, J. Davis and S. Thrun, "LidarBoost: Depth superresolution for ToF 3D shape scanning," in IEEE Conference Computer Vision and Pattern Recognition, Miami, 2009.
- [3] A. Makadia, "Fully automatic registration of 3D point clouds," in IEEE Conference Computer Vision and Pattern Recognition, New York, 2006.

- [4] T. Rabbani, F. A. van den Heuvel and G. Vosselman, "Segmentation of point clouds using smoothness constraint," in ISPRS Commission V Symposium Image Engineering and Vision Metrology, vol. 35, no. 6, pp. 248-253, Dresden, 2006.
- [5] R. B. Rusu, N. Blodow and M. Beetz, "Fast point feature histogram (FPFH) for 3D registration," in IEEE International Conference Robotics and Automation, pp. 1848-1853, Kobe, 2009.
- [6] R. B. Rusu, Z. C. Marton, N. Blodow and M. Beetz, "Learning Informative Point Classes for the Acquisition of Object Model Maps," International Conference Control Automation Robotics and Vision, Hanoi, 2008.
- [7] A. G. Buch, D. Kraft, J. K. Kamarainen, H. G. Petersen and N. Kruger, "Pose estimation using local structure-specific shape and appearance," in IEEE International Conference Robotics and Automation, pp. 2080-2087, Karlsruhe, 2013.
- [8] A. W. Fitzgibbon, "Robust registration of 2D and 3D point sets," Image and Vision Computing, vol. 21, no. 13, pp. 1145-1153, 2003.

Author Biography

Keisuke Myosen received the BS. degree from Chiba University in 2020. He is currently a master course student in Chiba University. He is interested in accurate 3D imaging.

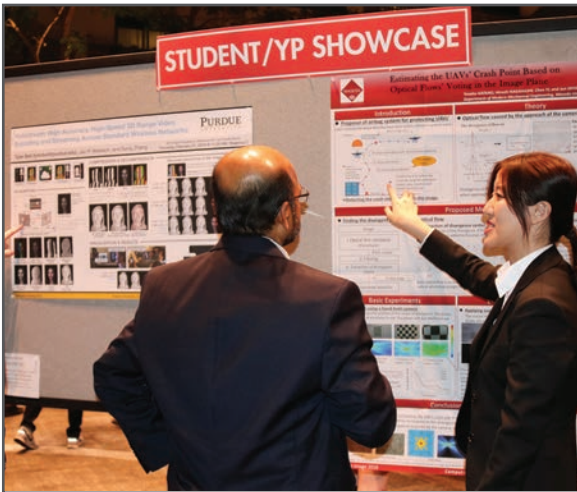
JOIN US AT THE NEXT EI!

IS&T International Symposium on

Electronic Imaging

SCIENCE AND TECHNOLOGY

Imaging across applications . . . Where industry and academia meet!



- **SHORT COURSES • EXHIBITS • DEMONSTRATION SESSION • PLENARY TALKS •**
- **INTERACTIVE PAPER SESSION • SPECIAL EVENTS • TECHNICAL SESSIONS •**

www.electronicimaging.org

